Polychaete trunk neuroectoderm converges and extends by mediolateral cell intercalation

Patrick R. H. Steinmetz*, Fabiola Zelada-González†, Carola Burgtorf, Joachim Wittbrodt, and Detlev Arendt‡

European Molecular Biology Laboratory, Developmental Biology Unit, Meyerhofstrasse 1, 69012 Heidelberg, Germany

Edited by John C. Gerhart, University of California, Berkeley, CA, and approved December 21, 2006 (received for review August 1, 2006)

During frog and fish development, convergent extension movements transform the spherical gastrula into an elongated neurula. Such transformation of a ball- into a worm-shaped embryo is an ancestral and fundamental feature of bilaterian development, yet this is modified or absent in the protostome model organisms *Caenorhabditis* or *Drosophila*. In the polychaete annelid *Platynereis dumerilii*, early embryonic and larval stages resemble a sphere that subsequently elongates into worm shape. Cellular and molecular mechanisms of polychaete body elongation are yet unknown. Our *in vivo* time-lapse analysis of *Platynereis* axis elongation reveals that the polychaete neuroectoderm converges and extends by mediolateral cell intercalation. This occurs on both sides of the neural midline, the line of fusion of the slit-like blastopore. Convergent extension moves apart mouth and anus that are both derived from the blastopore. Tissue elongation is actin-dependent but microtubule-independent. Dependence on JNK activity and spatially restricted expression of *strabismus* indicates involvement of the noncanonical Wnt pathway. We detect a morphogenetic boundary between the converging and extending trunk neuroectoderm and the anterior *otx*-expressing head neuroectoderm that does not elongate. Our comparative analysis uncovers striking similarities but also differences between convergent extension in the polychaete and in the frog (the classical vertebrate model for convergent extension). Based on these findings, we propose that convergent extension movements of the trunk neuroectoderm represent an ancestral feature of bilaterian development that triggered the separation of mouth and anus along the elongating trunk.

amphistomy | axis formation | convergent extension | gastrulation

An elongating worm-shaped body is characteristic for Bilateria. However, during their development, many bilaterians first resemble a sphere, which only later elongates into a worm shape (1, 2). For example, many crustaceans, annelids, and chordates that represent the three bilaterian superphyla (Ecdysozoa, Lophotrochozoa, and Deuterostomia) develop from a spherical blastula into the elongated form during and after gastrulation (3). During this process, the blastopore adopts its final position in the elongated animal to become mouth (protostomy), anus (in deuterostomy), or both mouth and anus (amphistomy). The study and comparison of body elongation in phylogenetically distinct bilaterian groups will contribute to our understanding of how the bilaterian body axes came into existence (1).

Vertebrate frogs and fishes develop a spherical blastula that, during gastrulation, transforms into an elongated neurula (4–7). This transformation is driven by convergent extension movements, the simultaneous narrowing and lengthening of the dorsal tissue (4–7). Similar morphogenetic movements were described in ascidians (8) and may also take place in amphioxus (9). Aside from chordates, however, little is known about the molecular and cellular mechanisms that underlie the elongation of spherical embryos and larvae. The nematode and fly model organisms are not well suited to fill that gap, because a spherical gastrula stage is modified or absent (10). Here we investigate axis elongation of the bristle worm *Platynereis dumerilii* (Polychaete, Annelida) as a contribution to the comparative study of body elongation in Bilateria. *Platynereis* appears particularly well suited for evolutionary comparisons, because it has retained an ancestral gene inventory and genome structure (11). As many other annelids [*Serpula* (12, 13), *Hydroïdes* (12), *Protula* (14), *Nereis* (15), and *Polygordius* (16)], *Platynereis* shows the amphistome mode of gastrulation with a slit-like blastopore giving rise to both mouth and anus (3).

Our work shows that during elongation of the spherical *Platynereis* trochophore larva into an elongated juvenile worm, the ventral trunk neuroectoderm undergoes convergent extension by actin-based mediolateral cell intercalation. This does not depend on cell divisions but requires JNK activity. We unravel a morphogenetic boundary between the converging and extending trunk neuroectoderm and the nonelongating head neuroectoderm that coincides with the molecular boundary between *gbx*- and *otx*-expressing body regions. Similarities and differences between polychaete and vertebrate convergent extension as well as possible implications for the evolution of the bilaterian body axes are discussed.

Results

***P. dumerilii* Undergoes Convergent Extension by Mediolateral Cell Intercalation.** In *Platynereis*, embryonic and larval stages exhibit a spherical shape to then transform into the elongated juvenile worm between 48 and 72 hours postfertilization (hpf) (Fig. 1*A*). We have documented elongation of the body axis in the neuroectoderm left and right of the neural midline (stippled black line in Fig. 1*A*). Using the early forming commissures and connectives of the axonal scaffold and the ciliary bands as morphological landmarks, we have determined that between 48 and 72 hpf, a defined rectangular piece of trunk neuroectoderm lengthens to 181 ± 5% and narrows to 49 ± 8% (along width II, Fig. 1*A*). Such reshaping of tissue is reminiscent of the convergent extension movements of the trunk neuroectoderm (and underlying mesoderm) in *Xenopus* (7, 17), chick (18), and zebrafish (5), which is driven, at least in large part, by polarized cell rearrangement such as mediolateral cell intercalation (19). This prompted us to investigate convergent extension movements of the polychaete neuroectoderm on the cellular level. Visualizing cellular outlines by a lipophilic dye and tracking individual cells by *in vivo* time-lapse imaging [Fig. 1 *B–E*, supporting information (SI) Fig. 5, and SI Movie 1], we observed polarized cell

Author contributions: P.R.H.S., J.W., and D.A. designed research; P.R.H.S., F.Z.-G., and C.B. performed research; P.R.H.S., F.Z.-G., C.B., J.W., and D.A. analyzed data; and P.R.H.S. and D.A. wrote the paper.

The authors declare no conflict of interest.

This article is a PNAS direct submission.

Abbreviations: hpf, hours postfertilization; p_{PTT}, paired Student's *t* test *P* value.

Data deposition: The sequences reported in this paper have been deposited in the European Molecular Biology Laboratory (EMBL) Nucleotide Sequence Database [accession nos. AJ505024 (*Pdu-gbx*), AM072762 (*Pdu-stbm*), AM072912 (*Pdu-alpha-tubulin*), and AM412058 (*Pdu-jnk*)].

*Present address: Sars International Centre for Marine Molecular Biology, Thormohlensgt. 55, N-5008 Bergen, Norway.

†Present address: Centre d'Immunologie Marseille-Luminy, Campus de Luminy, Case 906, F-13288 Marseille Cedex 09, France.

‡To whom correspondence should be addressed. E-mail: arendt@embl.de.

This article contains supporting information online at www.pnas.org/cgi/content/full/0606589104/DC1.

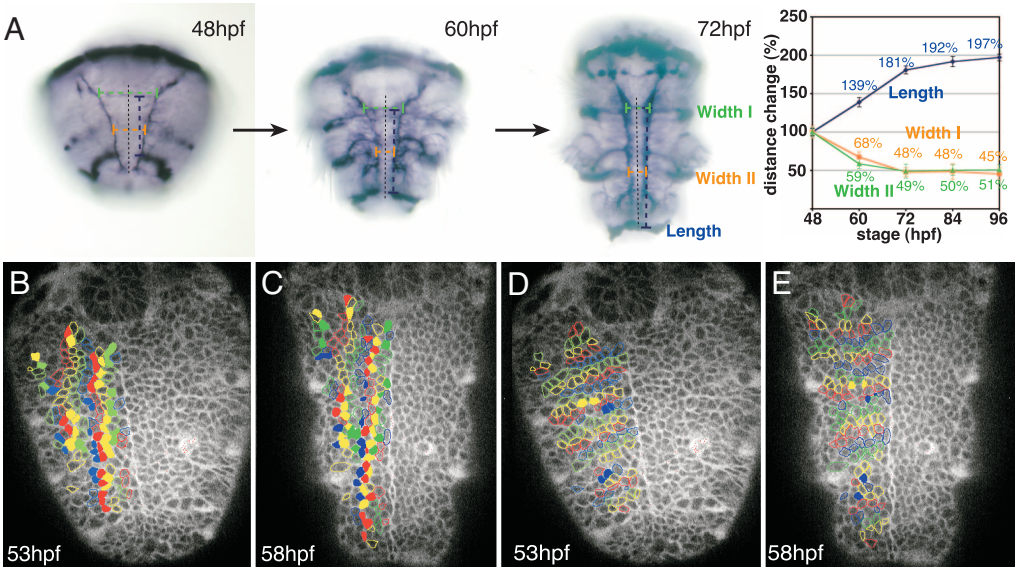

Fig. 1. Convergent extension in the *Platynereis* neuroectoderm by mediolateral cell intercalation. (*A*) Quantification of tissue transformation was done through morphological landmarks. Axonal scaffold and ciliary bands stained by antiacetylated α-tubulin antibody. The plotted distances in the graph refer to the colored dashed lines in the larvae. Note that axis elongation is almost complete at 72 hpf. Blue length, from poststomodaeal commissure to telotroch; green width I, between connectives at poststomodaeal level; orange width II, between connectives at level of second paratroch. Black stippled line, neural midline. (*B–E*) Cell intercalation events in mediolateral (*B* and *C*) and anteroposterior (*D* and *E*) direction. Frames of focal planes of a 300-min time-lapse recording between ≈53 and 58 hpf. Trackable cells are artificially colored in anteroposterior columns (*B* and *C*) or mediolateral rows (*D* and *E*). Filled cells depict tracked cells that are separated from one neighbor cell by at least one traced intercalating cell in mediolateral (*B* and *C*) or anteroposterior (*D* and *E*) direction.

rearrangement also in the *Platynereis* neuroectoderm where cells strongly intercalate in mediolateral direction (Fig. 1 *B* and *C*). In contrast, we hardly ever observed cells intercalating in anteroposterior direction (Fig. 1 *D* and *E*). Notably, *Platynereis* overall elongation by mediolateral cell intercalation is less pronounced than in the frog spinal cord (7) (exhibiting 12-fold elongation) but comparable in intensity to that in the medaka fish hindbrain (6) (exhibiting 2-fold elongation).

We next addressed whether mediolateral cell intercalation can fully account for the observed body elongation. One approach is to relate, for each given longitudinal column of cells within the converging and extending neuroectoderm, the percentage of total elongation [elongation index (17)] to the percentage of increase in cell number by mediolateral intercalation [mediolateral intercalation index (17)]. These percentages should not differ if mediolateral cell intercalation accounts for the observed elongation. In the 5-h period documented in Fig. 1 *B–E*, a given longitudinal column of cells on average increases in length to an elongation index of 129 ± 6% ($n = 6$), whereas the number of tracked cells that contribute to this column on average augments to a mediolateral intercalation index of 126 ± 14% ($n = 6$). This result indicates that mediolateral cell intercalation can fully account for the observed elongation but does not rule out that other factors, such as cell-shape changes, also contribute to a minor extent. To test for a possible contribution of cell shape change to convergent extension, we measured the lengths and widths of all cells tracked during the documented period and found no significant alterations [lengths to 104.8 ± 26% ($n = 139$); paired Student's t test P value (p_{PTT}) = 0.095; widths to 97.5 ± 32.1% ($n = 139$); $p_{PTT} = 0.37$]. In line with this, cell density (i.e., the number of cells in rectangles of constant surface area) did not change significantly [from 100.0 ± 7.9% ($n = 18$) to 100.7 ± 5.5% ($n = 17$); two-tailed Student's t test P value = 0.77].

Oriented Cell Division Does Not Contribute to Body Elongation. Because we occasionally observed dividing cells in our time-lapse recordings (SI Movies 1 and 2), we next tested whether cell division would also contribute to *Platynereis* body elongation as described for zebrafish (20) and chick (18). To this end, we prevented cytokinesis by arresting the cell cycle in the G_2/M phase with the microtubule-depolymerizing drug nocodazole. Incubating *Platynereis* larvae in nocodazole during elongation efficiently depolymerized microtubules, as evidenced by the absence of microtubule bundles in axon tracts (Fig. 2 *G* and *L Inset*), and produced various morphological defects (Fig. 2 *G* and *L*) but had no effect on body elongation in *Platynereis* (Fig. 2*A*). This observation rules out a major role not only for cell division but also for other microtubule-dependent cellular processes in elongating the *Platynereis* trunk neuroectoderm, corroborating our finding that mediolateral cell intercalation is the major driving force to elongate the *Platynereis* larval body. Note that *Xenopus* convergent extension is also insensitive to nocodazole, at least from stage 10.5 onwards (21–23).

In contrast, depolymerization of actin filaments by cytochalasin B incubation abolished convergent extension in a concentration-dependent manner (Fig. 2 *B*, *H*, and *L*), suggesting that mediolateral cell intercalation is driven by actin filament-based cellular processes, as described for the protrusive cells of the converging and extending *Xenopus* mesoderm (24) and neuroectoderm (17).

Expression of *Pdu-strabismus* and Inhibition of JNK. In vertebrates, activation of the noncanonical Wnt pathway is required for mediolateral cell intercalation (25). With the techniques at hands for *Platynereis*, we could analyze a possible involvement of the noncanonical Wnt pathway by expression analysis of the marker gene *strabismus* and by pharmacological inhibition of JNK acting further downstream in the same pathway in vertebrates (26) and *Drosophila* (27).

The transmembrane protein strabismus is a core member of a conserved group of proteins constituting the noncanonical Wnt pathway in *Drosophila* and vertebrates (28). We cloned the *Platynereis strabismus* gene (SI Fig. 6*A*) and indeed found it expressed in a restricted manner in the ventral neuroectoderm where mediolateral cell intercalation was observed (Fig. 2 *M* and *N*).

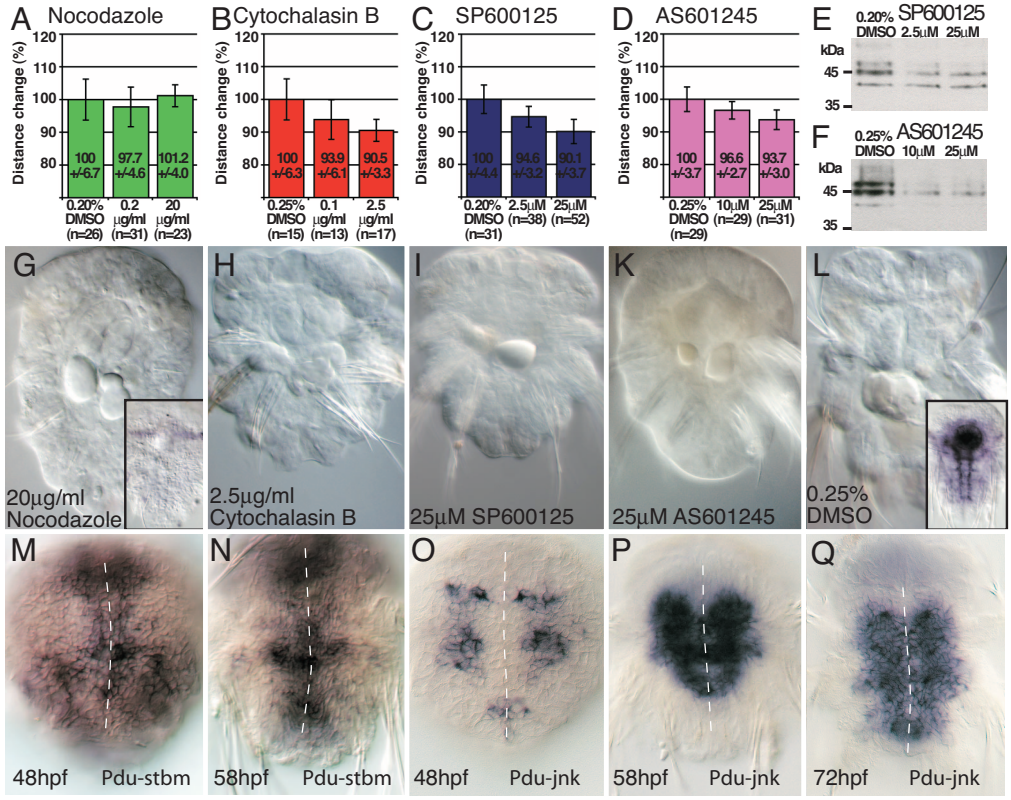

Fig. 2. Chemical inhibition experiments (*A–L*) and expression of *Pdu-strabismus* (*M* and *N*) and *Pdu-jnk* (*O–Q*). All treatments were done between 48 and 72 hpf except *E* and *F* (48–58 hpf). (*A*) Nocodazole treatment does not significantly reduce length at 0.2 μg/ml ($P = 0.13$) or 20 μg/ml ($P = 0.48$) compared with controls. (*B*) Cytochalasin B treatment significantly shortens larva in a concentration-dependent manner ($p_{0.1–2.5\mu g/ml} = 0.0493$) at 0.1 μg/ml ($P = 0.0115$) and 2.5 μg/ml ($P = 4.77 \times 10^{-6}$) compared with controls. (*C*) SP600125 treatment significantly shortens larva in a concentration-dependent manner ($p_{2.5–25\mu M} = 3.96 \times 10^{-9}$) at 2.5 μM ($P = 8.74 \times 10^{-8}$) and 25 μM ($P = 3.68 \times 10^{-18}$) compared with controls. (*D*) AS601245 treatment significantly shortens larva in a concentration-dependent manner ($p_{10–25\mu M} = 1.3 \times 10^{-4}$) at 10 μM ($P = 1.7 \times 10^{-4}$) and 25 μM ($P = 7.1 \times 10^{-10}$) compared with controls. Error bars represent standard deviations. Probabilities were calculated with two-tailed Student's *t* test assuming equal variance. (*E* and *F*) Western blots detecting phospho-JNK of embryos inhibited with SP600125 and AS601245 shows decreased autophosphorylation of JNK in comparison with 0.2% or 0.25% DMSO controls. Multiple bands may represent different JNK isoforms. A similar loading amount was controlled by Ponceau S staining (not shown). (*G–K*) Morphological defects after treatment with different inhibitors. (*G Inset*) Antibody staining of α-tubulin showing depolymerization of microtubules by the absence of characteristic staining in longitudinal axon bundles and mouth. (*L*) Control larva incubated in maximal concentration of organic solvent DMSO. (*L Inset*) Antibody staining of α-tubulin showing polymerized microtubules in longitudinal axon bundles and mouth. Dashed line, ventral midline. Ventral views; anterior is up.

JNK is required for convergent extension movements in vertebrates (26). Pharmacological inhibition of JNK thus represents a suitable test for the possible involvement of the noncanonical Wnt pathway in *Platynereis* convergent extension (although JNK is not restricted to that pathway; see, e.g., ref. 29). We cloned the *Platynereis jnk* gene (Fig. 6*B*) and found it strongly and specifically expressed in the ventral neuroectoderm (Fig. 2 *O–Q*). We treated larvae between 48 and 58 hpf with two chemically distinct inhibitors of JNK, SP600125 (30) or AS601245 (31) and found that the active autophosphorylated form of JNK (30) was strongly reduced in larval extracts, as evidenced by immunodetection of the conserved diphosphorylated Thr-Pro-Tyr epitope of JNK (Fig. 2 *E* and *F*) (32). Phenotypically, JNK inhibition resulted in a block of axis elongation (Fig. 2 *I*, *K*, and *L*), reproducing the effects seen after cytochalasin B incubation (Fig. 2 *B–D*, *H*, and *L*).

Expansion of the Neuroectodermal Surface Area. Mediolateral cell intercalation alone cannot expand the surface of the converging and expanding tissue. Still, we observed an overall expansion of the neuroectodermal surface area to 111 ± 14%, as evidenced by measuring average distances between tracked cells; we detected a distance increase along the longitudinal axis to 132.3 ± 2.9% ($n = 5$; $p_{PTT} = 6.7 \times 10^{-6}$) but a distance decrease along the mediolateral axis to 84 ± 10.8% ($n = 20$, $p_{PTT} = 6.0 \times 10^{-6}$) only. In the absence of significant cell shape and cell density changes (see above), this area increase should be due to the observed cell division (SI Movies 1 and 2) and/or radial cell intercalation (18).

The *Platynereis* neuroectoderm represents a multilayered epithelium (SI Fig. 7) that would allow radial intercalation of cells. Consistent with this assumption, we occasionally observed cells appearing in or disappearing from focal planes (SI Movie 1). Radial intercalation could not be further substantiated, because at the relevant stages, axonogenesis is long underway and produces a highly uneven basal surface curved around the axon tracts (SI Fig. 7 *I* and *II*), making it impossible to determine changes in neuroectodermal thickness.

Elongation of the Lateral and Dorsal Trunk Ectoderm. Because the *Platynereis* larva does not overtly bend, elongation of the lateral and dorsal body sides should approximate that of the ventral body side. We tracked cells on the lateral body side from 53.5 to 59.5 hpf and found that the average distance between cells along the longitudinal axis increased to 134.5 ± 11.1% ($n = 13$; $p_{PTT} = 9.9 \times 10^{-10}$), whereas that between cells along the dorsoventral axis of the larva decreased to only 95.2 ± 5.6% ($n = 9$; $p_{PTT} = 0.028$). Thus, elongation of the lateral body sides indeed closely

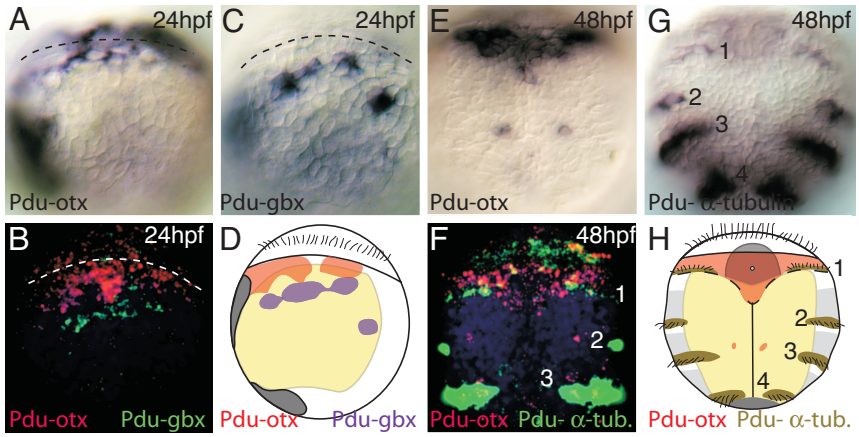

Fig. 3. The *otx–gbx* boundary in *Platynereis* larval morphology. Stained larvae after single color (*A*, *C*, *E*, and *G*) or fluorescent two-color whole-mount *in situ* hybridization (*B* and *F*). (*A–D*) Lateral views anteriorly tilted. (*D*) Schematized 24-hpf trochophore larva. (*E–H*) Ventral views anteriorly tilted. (*H*) Schematized 48-hpf trochophore correlating *Pdu-otx* expression (red) and the position of ciliary bands (brown). Numbers indicate position of ciliary bands. (*B and F*) Blue, nuclear DAPI staining. Yellow, neuroectoderm; light gray, invaginated cheatal sacs; dark gray, mouth and anal precursors.

matches that of the ventral body side, but they show only very little convergence. In line with this result, we observed a limited number of mediolateral cell intercalation events restricted to cells between the segmental pairs of appendages (SI Fig. 8 and SI Movie 2).

For technical reasons, we could not resolve the outlines of the very large and thin cells on the dorsal body side. We managed, however, to track individual dorsal cell nuclei (SI Fig. 9 and SI Movie 3) and determined that the average distance between them along the longitudinal axis increased to 140.0 ± 4.7% (n = 6; $p_{PTT} = 9.9 \times 10^{-6}$), whereas their average distance along the dorsoventral axis did not change significantly (to 91.5 ± 23.3%; n = 10; p_{PTT} = 0.16). We conclude that convergent extension is restricted to the ventral body side.

An *otx–gbx* Morphogenetic Boundary Anteriorly Delimitates the Converging and Extending Trunk Neuroectoderm. In vertebrates, convergent extension occurs in the prospective hindbrain and spinal chord neuroectoderm, whereas the fore- and midbrain neuroectoderm is devoid of these movements at open neural plate stages (6, 7). The boundary between these regions (the later midbrain–hindbrain boundary) is set at gastrula stages, where it is first apparent as a molecular boundary between the anterior *otx*-expressing region and the posteriorly adjacent stripe of *gbx* expression (33). In frogs, Otx has been shown to negatively regulate convergent extension movements through Calponin (34). A subdivision into an anterior *otx*- and a posteriorly adjacent *gbx*-expressing region is of widespread occurrence in developing bilaterians (1, 35–38), but a spatial correlation to the anteroposterior extent of convergent extension has not been documented except for vertebrates.

To investigate a possible correlation between the *otx–gbx* boundary and the anteroposterior extent of convergent extension movements in *Platynereis*, we analyzed the expression of the newly cloned *Pdu-gbx* (SI Fig. 10*E*) and the previously cloned *Pdu-otx* (39) by double-fluorescent whole-mount *in situ* hybridization (40). At 24 hpf, long before the onset of axis elongation in *Platynereis*, we observed a single transverse band of *Pdu-gbx*-expressing cells located posteriorly and not overlapping with the anterior *otx* expression territory (39) (Fig. 3 *A–D*). This molecular subdivision prevails into subsequent stages, with *Pdu-otx* being continuously expressed in anterior tissue surrounding the mouth opening (39) and *Pdu-gbx* in the trunk neuroectoderm (SI Fig. 10 *A–D*). Note that *Platynereis-gbx* expression later expands to more posterior trunk regions as also documented for *Xenopus* (41). This pattern resembles the pattern in *Drosophila* (35) and in amphioxus (42), where *gbx* is expressed more broadly in the trunk ectoderm.

To relate the molecular boundary between *Pdu-otx* and *Pdu-gbx* expression to larval morphology and morphogenesis, we costained for *Pdu-otx* and the ciliary marker *Pdu-α-tubulin* (Fig. 3 *E–H*). We could thus identify a band of cilia [representing the so-called "metatroch" (43), at the level of "1" in Fig. 3 *F–H*] that demarcates the posterior limit of *otx* expression from 48 hpf onwards (Fig. 3 *E–H*) and also represents the head–trunk boundary in polychaetes (44). The *otx–gbx* boundary thus corresponds to the head–trunk boundary in the *Platynereis* neuroectoderm. Because ciliated cells are also visible in the *in vivo* time-lapse recordings, we could follow this band of cilia (arrow in SI Fig. 11 *B* and *E*) through axis elongation and found that the *otx*-positive anterior tissue in front of this band narrows (SI Fig. 11*F*) but does not elongate (SI Fig. 11*C*). Convergent extension during elongation is therefore a characteristic feature of the developing ventral trunk and is absent in the head neuroectodem in *Platynereis*.

Discussion

Aside from vertebrates, convergent extension by cell intercalation has been described for different elongating tissues (e.g., *Drosophila* hindgut and Malpighian tubules, sea urchin archenteron, nematode dorsal ectoderm, and ascidian notochord; refs. 19 and 45). Axis elongation has been studied for the trochophore larva of various polychaetes such as *Polygordius* (16, 46), the terebellid *Amphitrite* (47, 48), the sabellids *Serpula* (49) and *Owenia* (50), the orbinid *Scoloplos* (51), and the nereidids *Nereis* (15) and *Platynereis* (52), but the underlying cellular mechanisms are unknown. Comparative annelid data exist for the directly developing leeches, where the trunk emerges and elongates by teloblastic stem cell proliferation (53, 54). However, leech axis elongation is different from that in polychaetes, at least at the cellular level. At the present state, it is thus unclear whether, and to what extent, the cellular mechanisms of axis elongation as documented here for the polychaete *Platynereis* is shared with other lophotrochozoans.

Yet, the comparison to vertebrate axis elongation reveals some unexpected and profound similarities at the level of tissue morphogenesis as well as at the cellular and molecular levels, as is exemplified for *Platynereis* and frog in Fig. 4 (and as also holds true for teleost fish). Both start from a spherical embryo/larva that is molecularly subdivided into a neural and a nonneural half (separated by stippled lines in Fig. 4 *A* and *C*) [the latter expressing *dpp/BMP2/4* orthologs (55); P.R.H.S. and D.A., unpublished data),

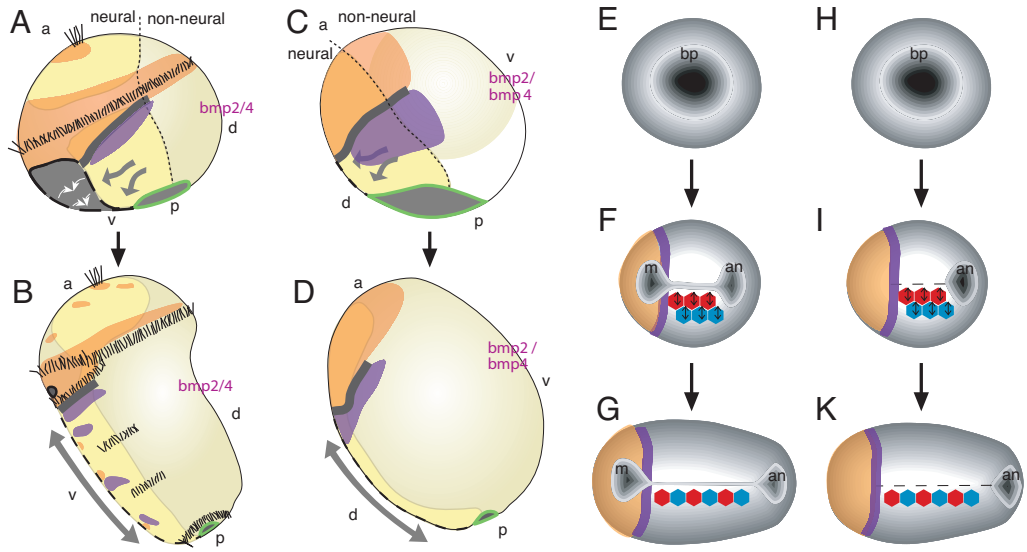

Fig. 4. The evolution of convergent extension movements and of the *otx–gbx* boundary in the context of amphistome and deuterostome gastrulation. (*A* and *B*) Schematic expression patterns of *Pdu-otx* and *Pdu-gbx* from stage 24 (*A*) to 72 hpf (*B*). White arrows, fusion of the lateral blastopore lips to form the neural midline. (*C* and *D*) Schematic expression patterns of *Xenopus laevis Xotx2* (38, 60) and *Xgbx2* (38, 41) from stage 11–11.5 (4, 7) (*C*) to stage 18 (4, 7) (*D*). Bold gray line, *otx–gbx* boundary; green outlines the presumptive anus; dashed lines, neural midline; stippled lines, border between neural and nonneural tissue; thick gray arrows, convergent extension movements of the neuroectoderm to extend the neural midline. Lateral views. (*E–K*) Convergent extension by mediolateral cell intercalation in an amphistome (*E–G*) and in a deuterostome (*H–K*). In the amphistome, mediolateral intercalation drives apart mouth (m) and anus (an). In the deuterostome, the slit-like blastopore no longer forms, but the corresponding movements persist. Vegetal views. Dashed line in *I* and *K*, neural midline. Yellow, neuroectoderm; orange, *otx*; purple, *gbx*. v, ventral; d, dorsal; a, anterior; p, posterior; an, anus; bp, blastopore; m, mouth.

and perpendicular to that, into *otx* and *gbx* regions (1, 35) (separated by bold gray lines in Fig. 4 *A–D*). The prospective neural midline is initially very short (Fig. 4 *A* and *C*, dashed line), so that the prospective anal cells (green line in Fig. 4 *A* and *C*) lie in close proximity to the anterior head neuroectoderm. The anus is then forced apart from the *otx*-expressing anterior head by the convergent extension movements (bold arrows in Fig. 4 *A–D*) along the neural midline, involving mediolateral cell intercalation. At the molecular level, mediolateral cell intercalation involves noncanonical Wnt signaling in frog and, possibly, also in *Platynereis.* In both species, these morphogenetic movements result in the formation of the neural body side, in the positioning of the anus at the posterior end, and in an overall elongation of the body. The overall complexity of this shared morphogenetic framework, where conserved transcription factors such as *otx* and *gbx* show similar restricted expression in corresponding tissues, suggests a common evolutionary origin.

Convergent extension of polychaetes and vertebrates, however, also shows an important difference that relates to the amphistome vs. deuterostome gastrulation modes, and that is illustrated in Fig. 4 *E–G* vs. Fig. 4 *H–K*. As is characteristic for amphistome gastrulation, the lateral blastopore lips fuse along the future neural midline separating the anterior mouth from the posterior anus (Fig. 4 *E–G*). Convergent extension then moves mouth and anus further apart from each other (Fig. 4 *F* and *G*), as is needed for the formation of a tube-shaped gut with an anterior mouth and posterior anus. The mouth territory itself is located anterior to the *otx–gbx* boundary and thus shifts anteriorly to become part of the head. In contrast, in vertebrates, the blastopore only gives rise to the anus (Fig. 4 *H–K*), and the convergent extension movements therefore entirely take place in front of the blastopore, which during gastrulation closes toward the posterior end of the elongating axis (Fig. 4*K*). Under the premise of an overall homology of polychaete and vertebrate trunk morphogenesis, these different patterns could be reconciled if vertebrate deuterostomy had evolved from an ancestral amphistome situation, as suggested (3, 56, 57) and as also put forward by the radial head hypothesis (1, 36). The vertebrate neural midline would then correspond to the line of fusion of the ancestral amphistome blastopore, and the ancestral mouth would have been lost in the course of dorsoventral axis inversion (58). Along these lines, we propose that convergent extension gastrulation movements and the *otx–gbx* morphogenetic boundary evolved in the context of amphistome gastrulation to set up the main bilaterian body axes with separate mouth and anus.

Conclusion

In a pioneer study on polychaete axis elongation, we have uncovered tissue rearrangements that very much resemble vertebrate convergent extension. Polychaete axis elongation involves mediolateral cell intercalation, requires JNK activity, and is anteriorly delimitated by the *otx–gbx* morphogenetic boundary. More comparative morphogenetic data will be needed for basal vertebrates such as lampreys, for other deuterostome groups such as cephalochordates and enteropneusts, and for other polychaetes, as well as for other lophotrochozoan groups, to explore the phylogenetic distribution of these strikingly similar patterns and to settle their significance for our understanding of the evolution of the bilaterian body axes.

Materials and Methods

Animal Culture. *Platynereis* larvae were obtained from an established breeding culture at the European Molecular Biology Laboratory.

Cloning of Genes. For all primers and various PCR conditions, see SI Table 1. Full-length clones of *Pdu-gbx* and *Pdu-strabismus* and partial clones of *Pdu-jnk* were isolated from *Platynereis* by nested PCR after reverse transcription of mRNA extracted from 24- or 48-hpf (*Pdu-stbm*) larvae. Full-length clones of *Pdu-gbx* and *Pdu-strabismus* were obtained by 5′- and 3′-RACE on an embryonic cDNA library of 24-, 48-, and 72-hpf larvae. Full-length clones of *Pdu-gbx* were obtained by fusion PCR by using cloned cDNA ends as template with vector-based T3 and T7 primers. *Pdu-stbm* 5′ ends

were amplified from a 48-h stage SMART RACE library (Clontech, Mountain View, CA). The 3′-cDNA end of *Pdu-stbm* was amplified from a 48-hpf cDNA library. *Pdu-α-tubulin* was identified during a sequencing screen of a 48-hpf EST library. Clone identities were confirmed by sequencing and orthology assignment based on multiple sequence alignments and neighbor-joining phylogenetic trees by using ClustalX (59).

Labeling of Cellular Outlines. Embryos were incubated for 15 min in 5 μM BODIPY564/570 coupled to propionic acid (Invitrogen, Carlsbad, CA) in natural seawater, then rinsed twice in natural seawater and mounted in a 1:1 mixture of natural seawater and 7.5% $MgCl_2$ to prevent muscular contractions.

Time-Lapse Recordings. Time-lapse recordings were performed with a PerkinElmer (Wellesley, MA) Ultraview RS System. Embryos were kept during recordings (12 frames per hour) at a constant temperature of 25°C or 26°C in natural seawater between slide and coverslip separated by two layers of adhesive tape and silicone paste. The chamber was sealed with mineral oil (Sigma, St. Louis, MO).

Image Analysis. Cell tracings and distance measurements used NIH Image 1.63 and ImageJ 1.32 and 1.33u. 3D reconstructions of the ventral plate used the Volume Viewer plugin for ImageJ.

Morphometric Measurements. Length and width measurements were made between the centers of two tracked cells. The change in surface area was measured by averaging surface area changes among five traced cells along the mediolateral axis and 20 traced cells along the anteroposterior axis. The elongation and mediolateral intercalation indices were measured as in ref. 17.

Incubations in Nocodazole, Cytochalasin B, SP600125, and AS601245. Embryos were incubated between 48 and 72 hpf in natural seawater containing Nocodazole (Sigma; 0.2 and 20 μg/ml), Cytochalasin B (Sigma; 0.1 and 2.5 μg/ml), SP600125 [A. G. Scientific (San Diego, CA); 2.5 and 25 μM], and AS601245 (Calbiochem, La Jolla, CA; 10 and 25 μM). Controls were incubated in 0.25% DMSO/natural seawater (except for Nocodazole, 0.2% DMSO).

Western Blotting. Embryos were incubated in either SP600125 or AS601245, lysed in 1× SDS sample buffer containing 1:100 phosphatase inhibitor mixture 1 (Sigma), boiled for 5 min at 100°C, vortexed, and homogenized by pulling up a syringe. Proteins were separated by SDS/PAGE and blotted onto a nitrocellulose membrane (Protran by Whatman, Brentford, U.K.). Similar protein loading was controlled by Ponceau S (Sigma). Phosphorylated JNK was detected by a Phospho-SAPK/JNK (Thr-183/Tyr-185) (1:400; Cell Signaling Technology, Beverly, MA) according to the manufacturer's protocol. A peroxidase-coupled goat anti-rabbit (Jackson ImmunoResearch, West Grove, PA) was used as secondary antibody and was detected with the ECL Detection Kit (Amersham, Piscataway, NJ).

Whole-Mount *in Situ* Hybridization and Immunohistochemistry. Embryos were fixed in 4% paraformaldehyde/1.75% PBS–Tween 20 for 2 h. Single-color and double-fluorescent whole-mount *in situ* hybridizations followed established protocols (40). Monoclonal antibodies were raised against acetylated α-tubulin (Sigma T6793; 1:250) and α-tubulin (Sigma clone DM1A; 1:500).

We thank Stephen Cohen (European Molecular Biology Institute) for critical reading of the manuscript, the members of the D.A. laboratory for help and discussion, Isabelle Philipp (University of California, Berkeley, CA) for a SP600125 protocol, M. Brand (Max Planck Institute of Molecular Cell Biology and Genetics, Dresden, Germany) for BODIPY564/570, and A. Nebreda [European Molecular Biology Laboratory (EMBL)] for a monoclonal α-tubulin antibody. We thank Jens Rietdorf, Stefan Terjung, and Timo Zimmermann (Advanced Light Microscopy Facility, Heidelberg, Germany; EMBL) for help in confocal microscopy techniques. This work was funded by a fellowship from the Luxembourg Ministry of Culture, Higher Education and Research (to P.R.H.S.)

1. Shankland M, Seaver EC (2000) *Proc Natl Acad Sci USA* 97:4434–4437.
2. Solnica-Krezel L (2005) *Curr Biol* 15:R213–R228.
3. Arendt D, Nübler-Jung K (1997) *Mech Dev* 61:7–21.
4. Keller RE (1975) *Dev Biol* 42:222–241.
5. Warga RM, Kimmel CB (1990) *Development (Cambridge, UK)* 108:569–580.
6. Hirose Y, Varga ZM, Kondoh H, Furutani-Seiki M (2004) *Development (Cambridge, UK)* 131:2553–2563.
7. Keller R, Shih J, Sater A (1992) *Dev Dyn* 193:199–217.
8. Munro EM, Odell G (2002) *Development (Cambridge, UK)* 129:1–12.
9. Conklin EG (1932) *J Morphol* 54:69–118.
10. Arendt D (2004) in *Gastrulation*, ed Stern C (Cold Spring Harbor Lab Press, Cold Spring Harbor, NY).
11. Raible F, Tessmar-Raible K, Oseogawa K, Wincker P, Jubin C, Balavoine B, Ferrier DE, Benes V, de Jong P, Weissenbach J, *et al.* (2005) *Science* 310:1325–1326.
12. Soulier A (1898) *C R Acad Sci* 126:1666–1669.
13. Conn HW (1884) *Zool Anzeiger* 7:669–672.
14. Soulier A (1899) *C R Acad Sci* 128:1591–1593.
15. Wilson EB (1892) *J Morphol* 6:361–480.
16. Woltereck R (1904) *Arch Entwick Org* 18:377–403.
17. Elul T, Koehl MA, Keller R (1997) *Dev Biol* 191:243–258.
18. Schoenwolf GC, Alvarez IS (1989) *Development (Cambridge, UK)* 106:427–439.
19. Keller R, Davidson L, Edlund A, Elul T, Ezin M, Shook D, Skoglund P (2000) *Philos Trans R Soc London B* 355:897–922.
20. Concha ML, Adam RJ (1998) *Development (Cambridge, UK)* 125:983–994.
21. Lane MC, Keller R (1997) *Development (Cambridge, UK)* 124:895–906.
22. Harris WA, Hartenstein V (1991) *Neuron* 6:499–515.
23. Kwan KM, Kirschner MW (2005) *Development (Cambridge, UK)* 132:4599–4610.
24. Shih J, Keller R (1992) *Development (Cambridge, UK)* 116:901–914.
25. Wallingford JB, Fraser SE, Harland RM (2002) *Dev Cell* 2:695–706.
26. Yamanaka H, Moriguchi T, Masuyama N, Kusakabe M, Hanafusa H, Takada R, Takada S, Nishida E (2002) *EMBO Rep* 3:69–75.
27. Boutros M, Paricio N, Strutt DI, Mlodzik M (1998) *Cell* 94:109–118.
28. Torban E, Kor C, Gros P (2004) *Trends Genet* 20:570–577.
29. Xia Y, Karin M (2004) *Trends Cell Biol* 14:94–101.
30. Bennett BL, Sasaki DT, Murray BW, O'Leary EC, Sakata ST, Xu W, Leisten JC, Motiwala A, Pierce S, Satoh Y, *et al.* (2001) *Proc Natl Acad Sci USA* 98:13681–13686.
31. Gaillard P, Jeanclaude-Etter I, Ardissone V, Arkinstall S, Cambet Y, Camps M, Chabert C, Church D, Cirillo R, Gretener D, *et al.* (2005) *J Med Chem* 48:4596–4607.
32. Sung YJ, Wu F, Schacher S, Ambron RT (2006) *J Neurosci* 26:6439–6449.
33. Rhinn M, Brand M (2001) *Curr Opin Neurobiol* 11:34–42.
34. Morgan R, Hooiveld MH, Pannese M, Dati G, Broders F, Delarue M, Thiery JP, Boncinelli E, Durston AJ (1999) *Nat Cell Biol* 1:404–408.
35. Hirth F, Kammermeier L, Frei E, Walldorf U, Noll M, Reichert H (2003) *Development (Cambridge, UK)* 130:2365–2373.
36. Bruce AE, Shankland M (1998) *Dev Biol* 201:101–112.
37. Rhinn M, Lun K, Amores A, Yan YL, Postlethwait JH, Brand M (2003) *Mech Dev* 120:919–936.
38. Tour E, Pillemer G, Gruenbaum Y, Fainsod A (2002) *Mech Dev* 112:141–151.
39. Arendt D, Technau U, Wittbrodt J (2001) *Nature* 409:81–85.
40. Tessmar-Raible K, Steinmetz PRH, Snyman H, Hassel M, Arendt D (2005) *BioTechniques* 39:460–464.
41. von Bubnoff A, Schmidt JE, Kimelman D (1996) *Mech Dev* 54:149–160.
42. Castro LF, Rasmussen SL, Holland PW, Holland ND, Holland LZ (2006) *Dev Biol* 295:40–51.
43. Nielsen C (2004) *J Exp Zool* 302B:35–68.
44. Schroeder PC, Hermans CO (1975) in *Reproduction of Marine Invertebrates*, eds Giese AC, Pearse JS (Academic, New York), Vol III, pp 1–213.
45. Keller R (2006) *Development (Cambridge, UK)* 133:2291–2302.
46. Hatschek B (1878) *Arb Zool Inst Wien TomI* 277–405.
47. Mead AD (1894) *J Morphol* 9:465–473.
48. Mead AD (1897) *J Morphol* 2:227–326.
49. Soulier A (1902) *Trav Inst Zool Monpellier Mem* 2:1–79.
50. Wilson DP (1932) *Philos Trans R Soc London B* 221:231–334.
51. Anderson DT (1959) *Q J Microsc Sci* 100:89–166.
52. Goette A (1882) *Abhandlungen zur Entwicklungsgeschichte der Würmer* (Voss, Leipzig, Germany).
53. Fernández J, Stent GS (1980) *Dev Biol* 78:407–434.
54. Weisblat DA, Harper G, Stent GS, Sawyer RT (1980) *Dev Biol* 76:58–78.
55. Holley SA, Jackson PD, Sasai Y, Lu B, De Robertis EM, Hoffmann FM, Ferguson EL (1995) *Nature* 376:249–253.
56. Siewing R (1985) *Lehrbuch der Zoologie Systematik* (Fischer, Stuttgart, Germany).
57. Naef A (1927) *Zool Jahrb Abt Anat Ontog Tiere* 49:357–390.
58. Arendt D, Nübler-Jung K (1994) *Nature* 371:26.
59. Thompson JD, Gibson TJ, Plewniak F, Jeanmougin F, Higgins DG (1997) *Nucleic Acids Res* 24:4876–4882.
60. Kablar B, Vignali R, Menotti L, Pannese M, Andreazzoli M, Polo C, Giribaldi MG, Boncinelli E, Barsacchi G (1996) *Mech Dev* 55:145–158.